

# Kinematic Design and Evaluation of a Six-Bar Knee-Ankle-Foot Orthosis

**Shramana Ghosh<sup>1</sup>**

Department of Mechanical and Aerospace Engineering,  
New York University,  
Brooklyn, NY 11201  
e-mail: sg5760@nyu.edu

**Nina P. Robson**

Department of Mechanical Engineering,  
California State University Fullerton,  
Fullerton, CA 92834  
e-mail: nrobson@fullerton.edu

**J. Michael McCarthy**

Department of Mechanical and Aerospace Engineering,  
University of California,  
Irvine, CA 92697  
e-mail: jmmccart@uci.edu

*This paper presents a new two-step design procedure and preliminary kinematic evaluation of a novel, passive, six-bar knee-ankle-foot orthosis (KAFO). The kinematic design and preliminary kinematic gait analysis of the KAFO are based on motion capture data from a single healthy male subject. Preliminary kinematic evaluation shows that the designed passive KAFO is capable of supporting flexion and extension of the knee joint during stance and swing phases of walking. The two-step design procedure for the KAFO consists of (1) computational synthesis based on user's motion data and (2) performance optimization. In the computational synthesis step, first the lower leg (knee-ankle-foot) of the subject is approximated as a 2R kinematic chain and its target trajectories are specified from motion capture data. Six-bar linkages are synthesized to coordinate the angular movements of knee and ankle joints of the 2R chain at 11 accuracy points. The first step of the design procedure yields 332 six-bar KAFO design candidates. This is followed by a performance optimization step in which the KAFO design candidates are optimally modified to satisfy specified constraints on end-effector trajectory and shape. This two-step process yields an optimally designed passive six-bar KAFO that shows promising kinematic results at the knee joint of the user during walking. The preliminary prototype manufactured is cost effective, easy to operate, and suitably demonstrates the feasibility of the proposed concept. [DOI: 10.1115/1.4046474]*

## 1 Introduction

Knee-ankle-foot orthosis (KAFOs) are lower extremity devices used to support the movement of knee joint in people with quadriceps muscle weakness [1]. Based on their primary functionality, KAFOs are broadly classified according to the design of their orthotic knee joints as: (1) conventional, (2) stance control, and (3) dynamic KAFOs [2]. Conventional KAFOs, which are passive devices, keep the knee joint of the device locked in extension throughout to provide stability to the user during walking [3]. The relative benefits of using a KAFO can be studied in terms of its: (1) kinematic gait quality measures, (2) patient satisfaction outcomes, and (3) energy consumption [4]. Kinematic gait quality measures, which will be the focus of this work, include speed of walking, step length, vertical displacement of center of mass, knee range of motion (ROM), etc. Due to the locked knee, conventional KAFOs result in altered gait patterns [3]. Stance control KAFOs (SC-KAFOs) lock the knee of the device during stance phase of walking to provide stability to the user and unlock it during the swing phase to allow the foot to clear the ground. SC-KAFOs can be both active (microprocessor-controlled knee joints that prevent its flexion during the stance phase) and passive (mechanical components such as ratchets and pawls, clutches, and cams, etc., lock and unlock the knee joint) [3–5]. This has been observed to result in more normal gait patterns compared to that obtained with conventional KAFOs [3]. Finally, dynamic KAFOs are devices that control the flexion and extension of the knee joint during both stance and swing phases by applying external torque throughout the whole gait cycle using an array of sensors and microprocessors and are active or externally powered devices [6]. These result in a more physiologically normal and safer gait for the user as compared to other types of KAFOs [2].

Dynamic KAFOs face several challenges including slow speed, high costs, and operational complexity [2,3]. SC-KAFOs are less

expensive but are noisy and bulky. They fail to provide ~70 deg of flexion required at the knee joint associated with physiologically normal walking [3]. Yet users walking with SC-KAFOs have demonstrably better kinematic outcomes in terms of speed, step length, and vertical displacement of center of mass as compared conventional KAFOs [7]. Conventional KAFOs are light weight, robust, inexpensive, and easy to operate; however, walking with them causes premature exhaustion to users as they need to adopt abnormal gait patterns to compensate for the locked knee [3]. Development of dynamic or active KAFOs to address the shortcomings of passive locked knee KAFOs or active and passive SC-KAFOs is an active area of research. Improvements in device design, reduction in weight, noisiness, complexity, and cost will increase their feasibility and accessibility. However, it is mechanically difficult to design compact knee joints that can assist physiologically normal motion during walking [5]. Thus, the challenge of designing orthoses that can improve kinematic gait outcomes over conventional KAFOs while providing similar robustness and ease of operation remains an open problem.

Some researchers have explored the feasibility of substituting single degree-of-freedom (DOF) linkages in place of bulky actuators in the design of robust orthoses. For example, Berkelman et al. [8] proposed a novel ankle-foot orthosis based on a passive four-bar linkage for people suffering from foot-drop disorder that results from injury to the central nervous system and causes dragging or slapping of the toe during walking. The assistive force required for ankle dorsiflexion is produced by the linkage mechanism which extends along the calf and foot and couples the motion of the knee and ankle joints. Single DOF mechanisms have also previously been used for the design of passive stationary gait rehabilitation machines such as a passive leg orthosis developed at the University of Delaware [9], the four-bar crank-rocker mechanism to obtain desired ankle trajectory presented by Ji and Manna [10], a 1DOF ten-bar mechanism to trace the trajectory of the toe presented by Tsuge and McCarthy [11], and a cam-linkage mechanism presented by Shao et al. [12]. Such gait rehabilitation mechanisms, however, cannot be used as orthoses due to their large sizes which would necessitate the need for additional supportive frameworks. The design of a crossed four-bar knee mechanism for a KAFO device was presented by Bapat and Sujatha

<sup>1</sup>Corresponding author.

Contributed by the Applied Mechanics Division Technical Committee on Dynamics & Control of Structures & Systems (AMD-DCSS) of ASME for publication in the JOURNAL OF ENGINEERING AND SCIENCE IN MEDICAL DIAGNOSTICS AND THERAPY. Manuscript received September 18, 2019; final manuscript received February 17, 2020; published online March 27, 2020. Assoc. Editor: Ping Zhao.

[13], that was optimally synthesized using genetic algorithms to mimic the instantaneous center of rotation of the human knee. However, no prototype design was presented of this work. A separate category of knee joints called polycentric or multi-axis knees are usually designed to replicate the instantaneous center of rotation of the anatomical knee joint. Polycentric knee joints with gears or cam mechanisms have been presented by Foster and Milan [14], Walker et al. [15], and Townsend and Knecht [16]. Of multi-axis knees composed of linkage-based mechanisms, four-bar knees are most common, as they are similar in structure to the human knee joint in the sagittal plane. Four-bar knee designs have been utilized extensively in the design of transfemoral prosthesis, and Radcliffe [17] documented the kinematic characteristics and advantages of such mechanisms.

However, all the devices and proposed designs mentioned previously only target a single joint or section of the lower leg of the user. In this work, our goal is to synthesize a linkage-based KAFO that produces better kinematic gait patterns as compared with passive conventional KAFOs and SC-KAFOs. The proposed KAFO will be robust, easy to use, and cost effective, by virtue of its design as a passive single DOF closed-loop linkage. It is intended that such a device could be used normally outside laboratory environments without supervision. To this end, we present a new two-step design procedure for single DOF KAFOs that consists of (1) computational synthesis based on user's motion data, and (2) performance optimization. The six-bar KAFO passively couples together the motion of the knee, ankle, and the foot throughout the entire gait cycle. A six-bar linkage is chosen for the design of the KAFO as it allows the coordination of a larger number of accuracy points (input–output angles) as opposed to four-bar linkages, and hence produces more complex motions [18]. Further, Plecnik and McCarthy [19] have demonstrated that Stephenson II six-bar function generators are well-suited to reproduce biomimetic motions such as that produced by the wings of a black-billed magpie. Plecnik and McCarthy [18] also designed a humanoid walker using three separate Stephenson II six-bar function generators to produce the input–output functions at the hip, knee, and ankle of the device. However, in order to provide robustness and stability to the six-bar KAFO by minimizing the number of moving parts, the designed device will only have a single six-bar linkage that will produce the walking gait. A preliminary six-bar KAFO linkage synthesis process was presented in Ref. [20]. However, the prototype developed was found to be difficult to operate by the user. Its kinematic performance is further discussed in Sec. 3.1.

Following the computational synthesis process, the linkages generated are kinematically optimized to generate more precise gait trajectories at the foot. Optimization is widely used for linkage synthesis, and a brief summary for optimization methods used for general mechanisms can be found in Smaili et al. [21], and for four- and six-bar linkages can be found in Tsuge et al. [22]. Tsuge et al. [22] rectified linkages that showed small deviations from the expected coupler trajectory using gradient-based optimization techniques. Constraints formulation based on concepts related to shape representations have been addressed by Dibakar and Mru-thyunjaya [23]. The two-step process illustrated here yields an optimally designed six-bar KAFO design candidate. Preliminary kinematic evaluation of the six-bar KAFO prototype shows prom-

ising quantitative kinematic results as compared to conventional KAFOs. To summarize, in this paper we present: (1) a new two-step kinematic design procedure for six-bar KAFO and (2) kinematic performance evaluation of passive KAFO prototype.

## 2 Methodology

**2.1 Step 1: Computational Synthesis Based on User's Motion Data.** The lower leg of a person can be kinematically modeled as a  $2R$  chain, where the knee joint is given by a fixed pivot  $B$ , the ankle joint by moving pivot  $F$ , and the distal end of the foot by a point  $P$  as shown in Fig. 1(a). For this work, the dimensions and target movements of the  $2R$  chain were specified using motion data from a test subject. The test subject or user is an adult healthy male, and required consent and permissions were obtained prior to performing the motion study. Motion data were obtained via a motion capture setup (Qualisys OptiTrack 4.2 (Qualisys North America, Inc., Highland Park, IL) consisting of seven infrared cameras (Qualisys Qqus500), located at the Human Interactive Robotics Laboratory at California State University Fullerton [24]. Accurate three-dimensional data representing the relative positions of the user's lower body were collected as they walked on a treadmill at a self-selected speed of 1.2 m/s. Segments of the leg, i.e., the thigh, shank, and foot, were each treated as separate rigid bodies. The motion of the lower leg in isolation was obtained by transforming the recorded motion data relative to a local frame fixed to the thigh segment. Figure 1(b) shows the target trajectory of the left foot relative to the fixed thigh frame.

A six-bar linkage can coordinate 11 accuracy points or input–output angle pairs [18]. The six-bar linkage used in this work was a Stephenson II six-bar linkage as shown in Fig. 2. Using a complex number notation for planar kinematics, the six-bar linkage was specified by the locations of its seven pivots, namely,  $A'$ ,  $B'$ ,  $C'$ ,  $D'$ ,  $F'$ ,  $G'$ , and  $H'$  in the reference position, i.e.,  $j = 0$ . Relative orientations of the moving links were measured from the reference position to the configuration of the linkage at the  $j$ th position, and were given by  $\Delta\phi_j = \phi_j - \phi_0$ ,  $\Delta\rho_j = \rho_j - \rho_0$ ,  $\Delta\psi_j = \psi_j - \psi_0$ ,  $\Delta\theta_j = \theta_j - \theta_0$  and  $\Delta\mu_j = \mu_j - \mu_0$  for  $j = 0, \dots, 10$ . Complex rotation operators were defined as

$$\begin{aligned} Q_j &= e^{i\Delta\phi_j} & S_j &= e^{i\Delta\psi_j} \\ R_j &= e^{i\Delta\rho_j} & T_j &= e^{i\Delta\theta_j} \\ U_j &= e^{i\Delta\mu_j} & & j = 1, \dots, 10 \end{aligned} \quad (1)$$

Locations of fixed pivots  $B'$  and  $F'$  were specified by designer based on the motion data of the user (refer to Fig. 3). The synthesis equations for the six-bar linkage were then used to find the locations of moving pivots  $A'$ ,  $C'$ ,  $D'$ ,  $G'$ , and  $H'$ . Normality conditions for the complex rotation operators are given by

$$\begin{aligned} R_j \bar{R}_j &= 1 & U_j \bar{U}_j &= 1 \\ T_j \bar{T}_j &= 1 & & j = 1, \dots, 10 \end{aligned} \quad (2)$$

Complex loop equations and corresponding complex conjugate loop equations for the six-bar linkage shown in Fig. 2 are

$$\begin{aligned} L_j : T_j (G' - C') &= [F' + Q_j (H' - F') + R_j (G' - H')] - [B' + S_j (C' - B')] \\ M_j : U_j (D' - A') &= [F' + Q_j (H' - F') + R_j (D' - H')] - [B' + S_j (A' - B')] \\ \bar{L}_j : \bar{T}_j (\bar{G}' - \bar{C}') &= [\bar{F}' + \bar{Q}_j (\bar{H}' - \bar{F}') + \bar{R}_j (\bar{G}' - \bar{H}')] - [\bar{B}' + \bar{S}_j (\bar{C}' - \bar{B}')] \\ \bar{M}_j : \bar{U}_j (\bar{D}' - \bar{A}') &= [\bar{F}' + \bar{Q}_j (\bar{H}' - \bar{F}') + \bar{R}_j (\bar{D}' - \bar{H}')] - [\bar{B}' + \bar{S}_j (\bar{A}' - \bar{B}')] \\ & \quad j = 1, \dots, 10 \end{aligned} \quad (3)$$

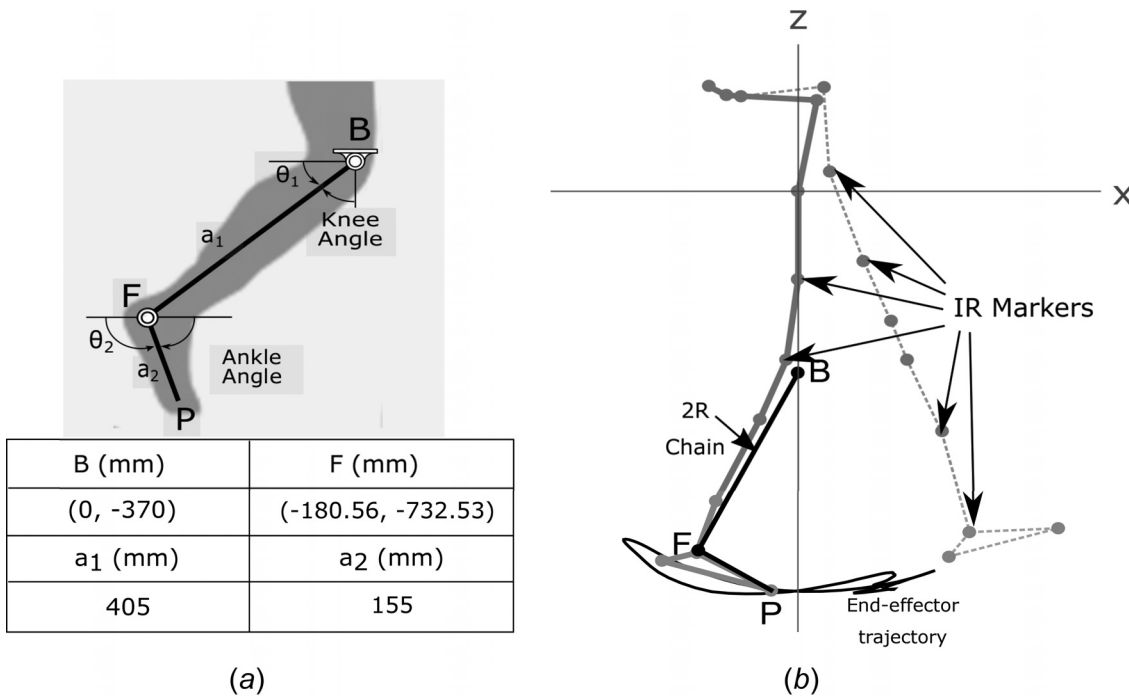


Fig. 1 (a) Kinematic model of the lower leg in the sagittal plane and (b) the trajectory traced by a marker placed at the distal end of the left foot of the user relative to a fixed thigh frame, and the 2R lower leg model chosen by the designer based on motion data of user

Equations (2) and (3) together form the synthesis equations for the Stephenson II six-bar function generator. For 11 accuracy points represented by  $j = 0, \dots, 10$ , a set of 70 equations in 70 unknowns are obtained, which can be reduced to a set of equations of degree 8 in 10 design parameters formed by  $A', C', D', G', H'$  and  $\bar{A}', \bar{C}', \bar{D}', \bar{G}', \bar{H}'$  as detailed in Ref. [18]. The total degree of the polynomial system is  $8^{10} = 1.07 \times 10^9$ . The general synthesis equations were solved by Plecník and McCarthy [18] using regeneration homotopy method with the open source software package BERTINI [25].

The goal of the computational synthesis step was to generate six-bar linkages which can couple the motion of the knee, ankle, and foot of the user during both the stance and swing phases of walking. The knee and ankle angular positions of the 2R chain lower leg were derived for any given position of point  $P$  by solving its inverse kinematics equations. Thus, 11 points were selected on user's walking trajectory, and their corresponding values of angles  $\theta_1$  and  $\theta_2$  were calculated. Finally, the six-bar linkage to be designed must be physically positioned such that it can couple the

motion of the knee, ankle, and foot of the user. Thus, the six-bar linkage was scaled and transformed as shown in Fig. 3. The angles  $\theta_1$  and  $\theta_2$  were then related to the input ( $\psi$ )—output ( $\phi$ ) angles required for the design task with a constant  $\beta$  which was eliminated by specifying the input and output angles as relative values with respect to the first task position, i.e.,  $\Delta\psi_k = \psi_k - \psi_0$  and  $\Delta\phi_k = \phi_k - \phi_0$ . Thus, the six-bar function generator coordinates, a set of 11 relative input–output angles, were given by

$$\begin{aligned}\Delta\psi_k &= -\Delta\theta_1 \\ \Delta\phi_k &= \Delta(\theta_2 - \theta_1) \quad k = 1, \dots, 10\end{aligned}\quad (4)$$

The 11 accuracy points selected and their corresponding input–output angles calculated are shown in Fig. 4 and enumerated in Table 1. The specific synthesis equations formulated were solved in 2 h, 14 min and 21 s on a single node of University of California, Irvine's high-performance computing cluster using the open source software package BERTINI [25]. Parallel processing was used with 64 CPUs at a speed of 2.2 GHz for each core. Further details can be found in Ref. [20].

**2.1.1 Computational Synthesis Results.** The computational synthesis process yielded 332 six-bar linkages. A preliminary screening process showed that nine of the 332 synthesized linkages passed through ten out of the 11 accuracy points specified in step one of the design procedure, 90 linkage candidates passed

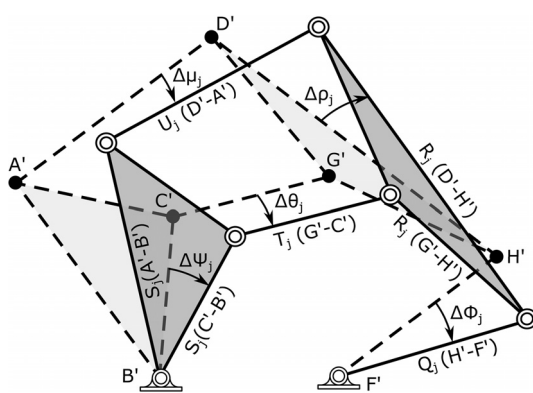


Fig. 2 A Stephenson II six-bar linkage, shown in its initial configuration (dashed lines) and  $j$ th configuration (solid lines) (adapted from Ref. [18])

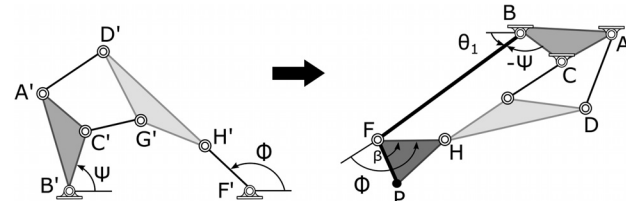


Fig. 3 Transformed six-bar function generator attached to a 2R serial chain that represents the user's lower-leg

through nine of the 11 specified points, and 233 linkages passed through eight of the 11 specified positions. None passed through all 11 accuracy points. Additionally, six of these linkages were found to be free of order defects, i.e., they moved through the accuracy points in the order specified by the designer. These six linkages are the design candidates for KAFOs and shown in Fig. 5. An examination of design candidates 3 and 4 show nonclosure of the metatarsal or end-effector trajectory and moving pivot  $G$  of design candidate 2 is found to have a section of its end-effector trajectory below ground level. Solution 6 passes through only nine of the specified eleven points. Thus, solutions 1 and 5 were found to be the most suitable design candidates. A preliminary prototype of linkage 1 was built and tested with the user [20,26]. A computer-aided design model of the designed device and the manufactured prototype are shown in Fig. 6.

**2.2 Step 2: Performance Optimization.** The computational formulation can be solved for only 11 accuracy points. Through optimization, the designer can evaluate the kinematic performance of the linkage at a larger set of task positions, hence reducing the importance of selecting the accuracy points for success of a design task. In order to obtain closer coupling of knee and ankle motion with the user's walking trajectory, the design candidates obtained through the computational synthesis step were optimally modified in the second step. The user's motion data consisted of 116 data points for the position of the foot captured during a single gait cycle. A basis spline was defined with the 116 data points as control points. A set of 50 points were selected to form the target walking trajectory to be used for the optimization process and shown in Fig. 7.

The computational synthesis solutions were grouped together based on proximity of their pivot locations, as members of each group displayed similar kinematic characteristics. Based on this observation, it was hypothesized that exploring regions in the vicinity of design solutions from step 1 could lead to identification of optimal linkage solutions that meet the design criterion. Thus, design solutions from step 1 were used to specify initial values of the design vector,  $X$ . Fixed pivots  $B$  and  $F$  were colocated with the knee and ankle joints of the user, respectively, and were invariant. A sensitivity analysis showed that variation in locations of pivots  $D$ ,  $G$ , and  $H$  did not result in significant changes to the value of the objective function. Thus, only the two pivots  $A$  and  $C$  were varied to reduce the computational time of the optimization step. Additionally, the benefit of varying only pivots  $A$  and  $C$  were that their locations could be modified without completely disassembling the mechanism. It offers the benefit of allowing the user to reconfigure the device to obtain optimal performance without reassembling the entire mechanism. The final design variable vector  $X$  consists of

$$X = (A, C)^T \quad (5)$$

**2.2.1 Error Function.** In order to generate the maximum assistive forces to support the motion of the knee during walking, the goal of this optimization process was to minimize the deviation of a given six-bar linkage from the target walking trajectory of the foot. The error function quantitatively measured the deviation of the end-effector of a six-bar linkage from the user's walking trajectory. If a point  $P_j$  on the user's walking trajectory also lay on the end-effector trajectory of the six-bar linkage shown in Fig. 8, it would satisfy the following loop equations:

$$\begin{aligned} T_j(G - C) &= -R_j(H - G) - Q_j(P_0 - H) + (P_j - C) \\ \bar{T}_j(\bar{G} - \bar{C}) &= -\bar{R}_j(\bar{H} - \bar{G}) - \bar{Q}_j(\bar{P}_0 - \bar{H}) + (\bar{P}_j - \bar{C}) \\ U_j(D - A) &= -R_j(H - D) - Q_j(P_0 - H) + (P_j - A) \\ \bar{U}_j(\bar{D} - \bar{A}) &= -\bar{R}_j(\bar{H} - \bar{D}) - \bar{Q}_j(\bar{P}_0 - \bar{H}) + (\bar{P}_j - \bar{A}) \end{aligned} \quad (6)$$

The rotation operators  $T_j$  and  $U_j$  were eliminated from Eq. (6) by multiplying each equation with its complex conjugate

$$\begin{aligned} |G - C|^2 &= |R_j(H - G) + Q_j(P_0 - H) - (P_j - C)|^2 \\ |D - A|^2 &= |R_j(H - D) + Q_j(P_0 - H) - (P_j - A)|^2 \\ &\quad j = 1, \dots, N - 1 \end{aligned} \quad (7)$$

The value of the rotation operator  $Q_j$  for a point  $P_j$  on the desired trajectory was found using

$$\begin{aligned} S_j(F - B) + Q_j(P_0 - F) &= P_j - B \\ \bar{S}_j(\bar{F} - \bar{B}) + \bar{Q}_j(\bar{P}_0 - \bar{F}) &= \bar{P}_j - \bar{B} \\ S_j \bar{S}_j &= 1 \\ Q_j \bar{Q}_j &= 1 \quad j = 1, \dots, N - 1 \end{aligned} \quad (8)$$

Equation (8) was simplified by eliminating  $S_j$  and  $\bar{S}_j$  by using the relationship  $S_j \bar{S}_j = 1$  to yield

$$\begin{aligned} (\bar{P}_j - \bar{B})(P_0 - F)Q_j + (F - B)(\bar{F} - \bar{B}) - (P_j - B)(\bar{P}_j - \bar{B}) \\ - (P_0 - F)(\bar{P}_0 - \bar{F}) + (P_j - B)(\bar{P}_0 - \bar{F})\bar{Q}_j &= 0 \\ &\quad j = 1, \dots, N - 1 \end{aligned} \quad (9)$$

As  $Q_j \bar{Q}_j = 1$ , Eq. (9) could also be written in the following quadratic form:

$$aQ_j^2 + bQ_j + c = 0 \quad j = 1, \dots, N - 1 \quad (10)$$

where

$$\begin{aligned} a &= (\bar{P}_j - \bar{B})(P_0 - F) \\ b &= (F - B)(\bar{F} - \bar{B}) - (P_j - B)(\bar{P}_j - \bar{B}) - (P_0 - F)(\bar{P}_0 - \bar{F}) \\ c &= (P_j - B)(\bar{P}_0 - \bar{F}) \end{aligned}$$

Given the numerical values of  $Q_j$  corresponding to each value of  $P_j$ , the numerical values of the rotation operator  $R_j$  and its conjugate  $\bar{R}_j$  were solved for using Eq. (7). The following substitutions were then introduced to simplify the equations:

$$\begin{aligned} a &= a_x + ia_y = H - G \\ b_j &= b_{xj} + ib_{yj} = Q_j(P_0 - H) - P_j + C \\ c &= c_x + ic_y = H - D \\ d_j &= d_{xj} + id_{yj} = Q_j(P_0 - H) - P_j + A \\ f &= f_x + if_y = G - C \\ g &= g_x + ig_y = D - A \quad j = 1, \dots, N - 1 \end{aligned} \quad (11)$$

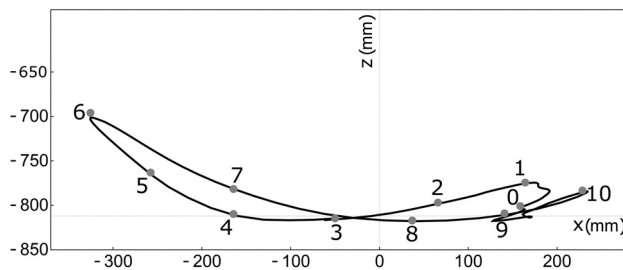


**Fig. 4 The 11 specified task points on the user's walking motion data**

**Table 1** Coordinates of point  $P$  on the target walking trajectory selected for linkage synthesis, and the corresponding values of  $\Delta\psi$  and  $\Delta\phi$ , the input and output angles of the six-bar function generator

Task position #	$P$ (mm)	$\Delta\psi$ (rad)	$\Delta\phi$ (rad)	Task position #	$P$ (mm)	$\Delta\psi$ (rad)	$\Delta\phi$ (rad)
0	(155.56, -799.66)	0	0	6	(-326.33, -697.47)	1.12	-0.04
1	(165.21, -774.79)	-0.02	0.14	7	(-163.13, -781.99)	0.74	-0.10
2	(67.46, -797.2)	0.22	0.17	8	(38.50, -816.88)	0.27	0.06
3	(-49.03, -814.55)	0.47	0.07	9	(141.99, -808.93)	0.03	-0.03
4	(-162.88, -809.67)	0.69	-0.09	10	(229.62, -783.63)	-0.18	-0.12
5	(-256.86, -763.49)	0.91	-0.10				

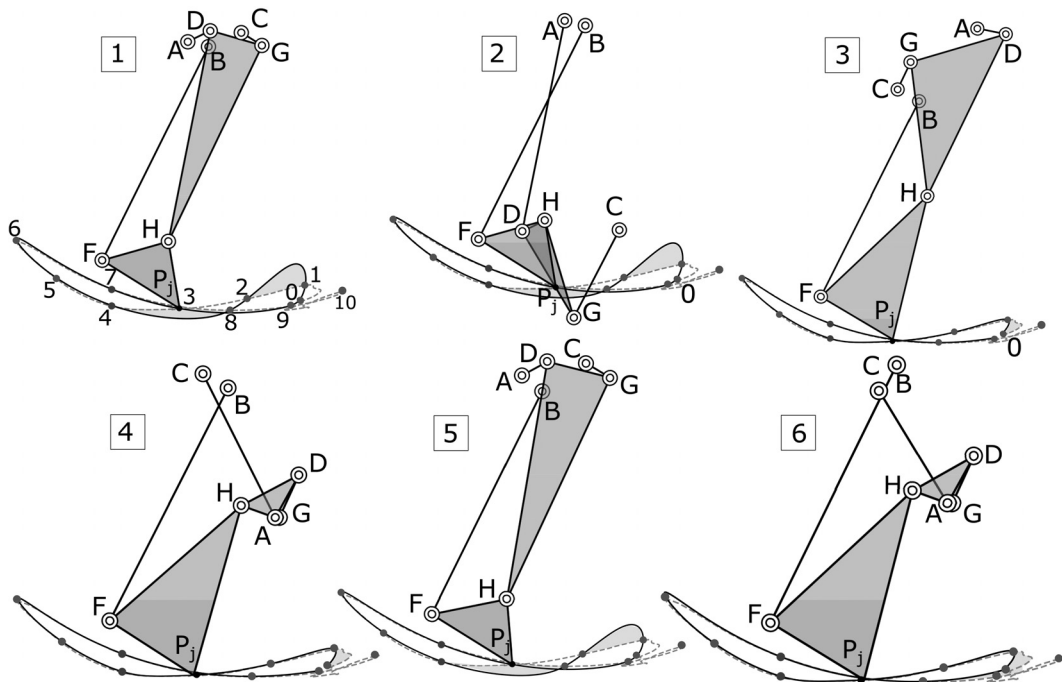


**Fig. 5** KAFO design candidates obtained from the computational synthesis process



**Fig. 6** (a) Computer-aided design model of prototype of KAFO device based on linkage solution 1 and (b) the corresponding manufactured prototype

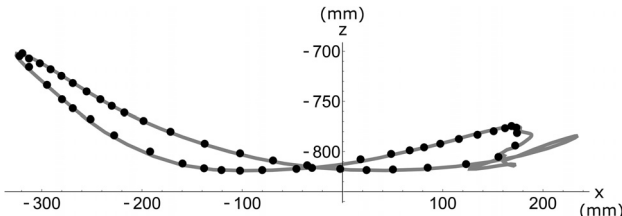


**Fig. 7** The target walking trajectory for performance optimization, defined as a set of 50 points, obtained from a basis spline of the motion data of the user

Substituting into Eq. (7)

$$\begin{bmatrix} a\bar{b}_j & \bar{a}\bar{b}_j \\ c\bar{d}_j & \bar{c}\bar{d}_j \end{bmatrix} \begin{bmatrix} R_j \\ \bar{R}_j \end{bmatrix} = \begin{bmatrix} f\bar{f} - a\bar{a} - b_j\bar{b}_j \\ g\bar{g} - c\bar{c} - d_j\bar{d}_j \end{bmatrix} \quad j = 1, \dots, N-1 \quad (12)$$

Which is a system of linear equations and were solved by using Cramer's rule. If the calculated values of  $R_j$  and  $\bar{R}_j$  satisfied the relationship  $R_j\bar{R}_j = 1$ , i.e., they were conjugates of each other, then point  $P_j$  lay on the end-effector of the linkage defined by the pivots  $(A, B, C, D, F, G, H, P_0)$ . The deviation of a given linkage from the user's target walking trajectory was thus quantitatively defined as

$$Err(X) = \sum_{k=1}^N R_k(X)\bar{R}_k(X) - 1 \quad (13)$$

**2.2.2 Closure of Metatarsal Trajectory.** It was essential that the end-effector of any six-bar linkage traced a closed metatarsal trajectory as the device moves through one gait cycle to be considered as a KAFO design candidate, i.e.,  $P_0 = P_{N-1}$ . Closure of the end-effector trajectory was verified by checking for existence of real-valued end-effector points as six-bar linkages completed one gait cycle. If a real-valued end-effector point was not found by solving the forward kinematics equations for the linkage, a penalty  $W_c$  was imposed. Additionally, the Euclidean distance between real-valued end-effector points for crank angle  $\theta_0 = 0$  deg and  $\theta_{N-1} = 360$  deg was calculated. Nonzero value of  $|P_0 - P_{N-1}|$  indicated open trajectory and an additional penalty of  $W_c \times |P_0 - P_{N-1}|$  was imposed. The penalty for nonclosure the metatarsal trajectory was given as

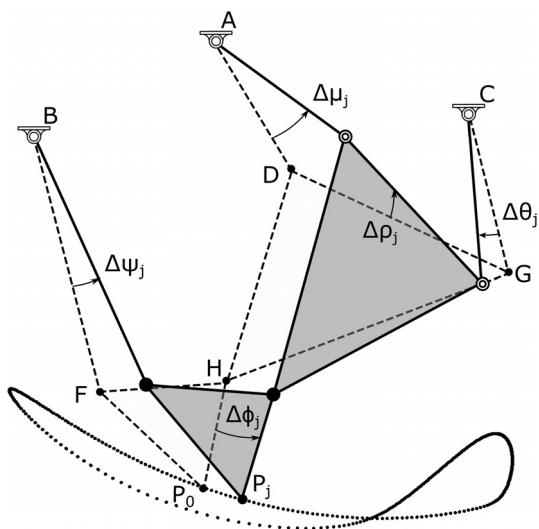


**Fig. 8** A six-bar linkage, shown in its initial configuration (dashed lines) and  $j$ th configuration (solid lines) (adapted from Ref. [22])

$$M_c = |P_0(X) - P_{N-1}(X)| + \sum_{i=0}^{N-1} g_c(P_i(X)) \quad (14)$$

where  $g_c(x + iy) = \begin{cases} 0 & \text{if } x \text{ and } y \text{ are real} \\ 1 & \text{if } x \text{ and } y \text{ are not real} \end{cases}$

**2.2.3 Continuity Between Trajectory Points.** Nonsmooth mechanical advantage curve having values of Jacobian determinant close to zero ( $\pm 10^{-4}$ ) would result in jerky movements that would affect the kinematic performance of the KAFO device and cause injury to the user. Thus, it was penalized by a factor of  $W_j$  according to the following function:

$$M_b = g_j(\det(J_j(X))) \quad \text{where } g_j(x) = \begin{cases} 0 & \text{if } x \leq 10^{-4} \\ 1 & \text{if } x > 10^{-4} \end{cases} \quad (15)$$

**2.2.4 Minimum Position and Orientation Mismatch.** It was necessary to minimize the deviations in the location and orientation between the end-effector trajectory of six-bar linkage solutions and the user's walking trajectory specified from motion data. To do this, bounding boxes were specified around linkage end-effector trajectory, such that the corners of the box were denoted by  $(C_{x_{\min}}, C_{y_{\min}})$  and  $(C_{x_{\max}}, C_{y_{\max}})$ . Similarly, the corners of the target curve bounding box were given by  $(T_{x_{\min}}, T_{y_{\min}})$  and  $(T_{x_{\max}}, T_{y_{\max}})$ . Then, from Fig. 9, the penalty for mismatch between position and orientation mismatch between target and linkage trajectory was given by

$$M_{tc} = \left( (T_{x_{\max}} - C_{x_{\max}}(X))^2 + (T_{y_{\max}} - C_{y_{\max}}(X))^2 \right. \\ \left. + (T_{x_{\min}} - C_{x_{\min}}(X))^2 + (T_{y_{\min}} - C_{y_{\min}}(X))^2 \right)^{1/2} \quad (16)$$

**2.2.5 Objective Function.** The optimization problem was expressed as a weighted objective function using penalties as

$$\min_{(X)} \left\{ \left[ \sum_{k=0}^{N-1} R_k(X)\bar{R}_k(X) - 1 \right] + W_c \times M_c + W_j \times M_j + W_{tc} \times M_{tc} \right\} \quad (17)$$

**2.2.6 Grid Search Algorithm.** Derivative-based optimization methods were not found to be appropriate for this problem as the constrained objective function had nondifferentiable regions in the solution space. Thus, derivative-free methods, also called direct search algorithms, which test the objective function at points generated based on algorithm-specific rules were used [27]. Tests with derivative-free optimization algorithms, namely Nelder–Mead, simulated annealing, differential evolution and random search in Mathematica [28], failed to converge to real solutions for this problem. A direct search was then conducted in the vicinity of the pivots A and C of the computational synthesis solutions using a grid search algorithm. Even though generating a sequence of grid points is trivial, this method faced a problem as

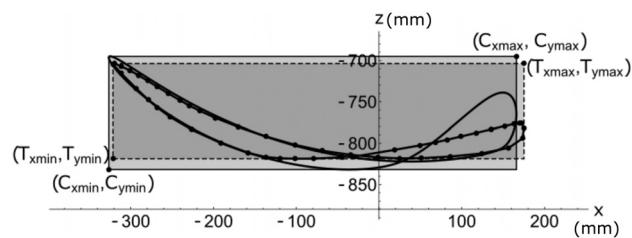


**Fig. 9** Bounding boxes of the linkage end-effector trajectory (solid line) and the user's target walking trajectory (dashed line)

**Table 2 Design parameters of the optimal design solutions 1, 4, and 5 compared with their initial values**

Pivot	Initial design 1 (mm)	Optimal solution 1 (mm)	Initial design 4 (mm)	Optimal solution 4 (mm)	Initial design 5 (mm)	Optimal solution 5 (mm)
A	(-35.05, -361.37)	(-38, -365)	(79.51, -57.85)	(81, -570)	(-33.11, -344.42)	(-34, -347)
C	(55.98, -345.67)	(57, -345)	(-38.95, -347.93)	(-34, -343)	(71.5, -323.96)	(72, 323)

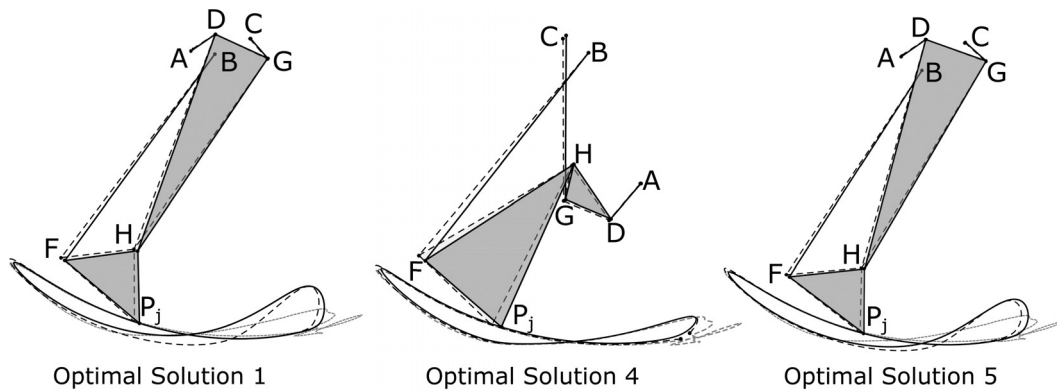


**Fig. 10** Comparison of metatarsal trajectory of the linkage obtained by optimally modifying linkage solutions 1, 4, and 5. Gray lines show experimental data corresponding to unassisted walking, dashed black lines represent the kinematic behavior of the initial designs, while solid black lines represent kinematic behavior of the optimal solutions.

the computational time was exponentially related to the number of elements in the design variable vector  $X$ . A grid with  $N = 20$  points in one dimension required the evaluation of the objective function at  $20^4 = 160,000$  points. We generated a  $20 \times 20$  mm grid with a step size of 1 mm centered about the initial pivot locations for each viable linkage candidate obtained from the computational synthesis process. The objective function was evaluated at each point, and a four-dimensional vector with the smallest objective function value was returned.

**2.3 Performance Optimization Results.** The grid search process successfully found three optimized design candidates that had lower values of the objective function formulated as

compared to the initial design solutions produced by the computational design process. The optimal design parameters obtained for the three optimized linkage solutions are presented in Table 2. Figure 10 shows the optimized linkages and their generated trajectories as compared to the initial designs. The error function maintained the angular relationship between the knee and ankle joints, while the penalties imposed reduced deviations from the user's target walking trajectory. The penalty imposed for nonclosure of metatarsal trajectory was successful in guiding the optimization procedure in finding pivot locations for design candidate 4 that closed the metatarsal trajectory. The effect of the penalty imposed on mismatch between the position and orientation of the metatarsal trajectory resulted in a closer match of the metatarsal trajectory of optimal solution 1 with the desired trajectory. Optimal design



**Fig. 11** Final prototype of the KAFO device

solution 4 was selected for design of the KAFO device as it has a more desirable ankle angle movement in the stance phase, as well as a closer match with the desired metatarsal trajectory. The manufactured device prototype is shown in Fig. 11.

### 3 Results

**3.1 Performance Analysis of Preliminary Prototype Based on Results of Computational Synthesis.** To conduct a preliminary performance analysis of the prototype constructed using linkage solution 1 from the computational synthesis process, motion capture data of the test subject walking on level ground with and without the six-bar KAFO prototype was obtained. Figure 12(a) illustrates the metatarsal trajectory of the user's foot over a complete gait cycle, as well as the knee and ankle angular motion for the following three cases (1) motion data of user walking normally without any assistance, (2) calculated kinematics of linkage

solution 1, and (3) motion data of the user walking with the preliminary prototype of the six-bar KAFO device. The user's knee ROM was found to be 61.89 deg with the preliminary prototype. In addition, stride length with the preliminary prototype was found to be 97% of stride length observed during unassisted locomotion. However, at the ankle joint, the user's ROM was found to be 52.62 deg when walking with the preliminary prototype as opposed to their ROM of 21.46 deg for unassisted walking. Maximum deviations from desired ankle angular behavior were observed during early stance phase due to excessive plantar flexion and in the swing phase due to excessive dorsiflexion. The six-bar linkage couples knee, ankle, and foot of the user, and the maximum ankle angular deviations were found to correspond to the maximum end-effector trajectory deviations. Thus, it was hypothesized that the excessive angular movement at the ankle joint was the result of compensatory actions taken by the user to counterdeviations in the end-effector trajectory of preliminary prototype from normal walking trajectory.

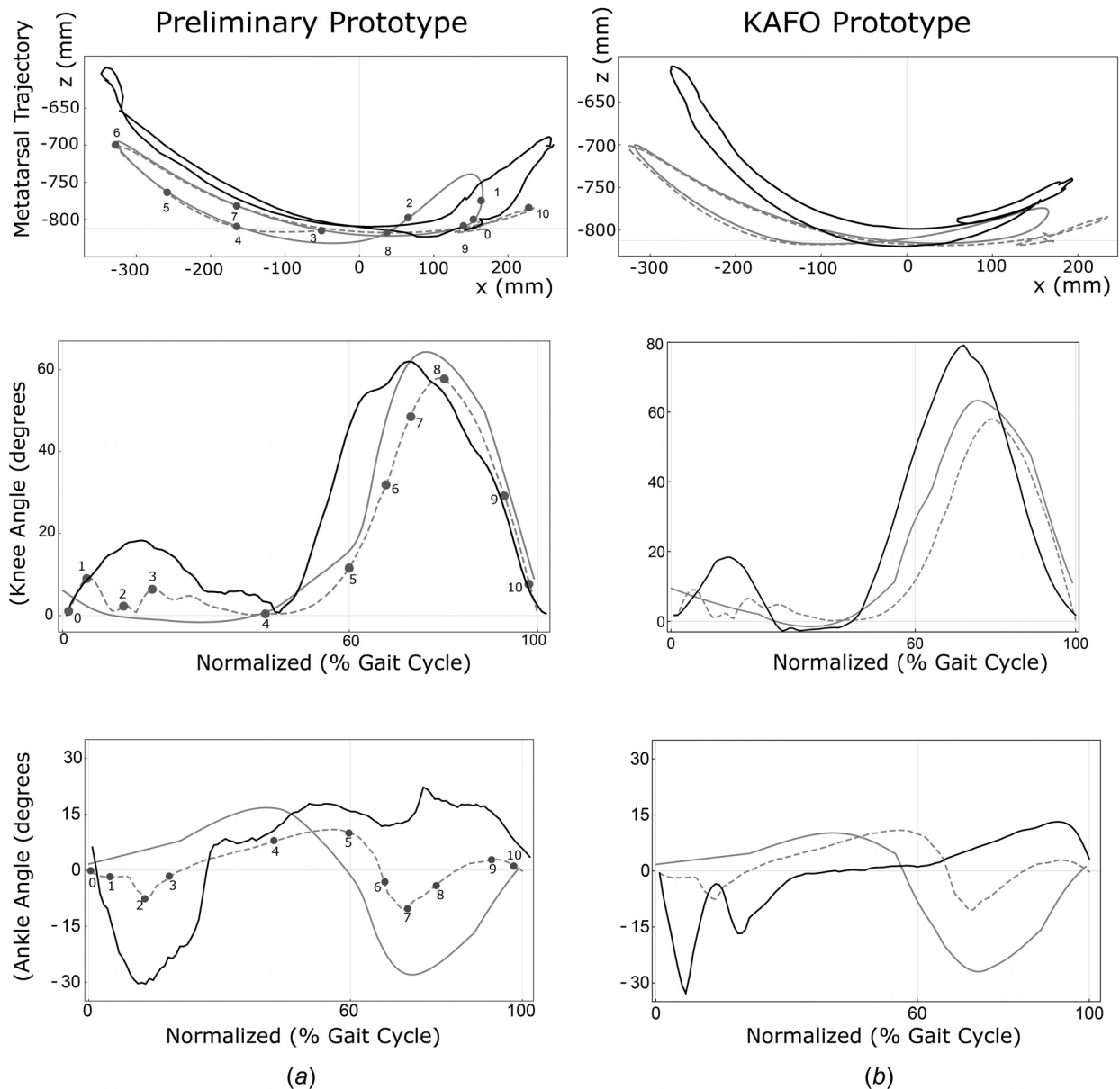


**Fig. 12 Comparison of metatarsal trajectory and knee and ankle joint angles of the user walking with (solid black lines) and without (dashed gray lines) the (a) preliminary prototype and (b) final prototypes of the KAFO compared with kinematic design predictions (solid gray lines)**

**3.2 Performance Analysis of Final Six-Bar Knee-Ankle-Foot Orthosis Prototype.** For performance analysis of the final KAFO prototype, motion data is collected of the test subject walking on level ground with and without the final six-bar KAFO prototype at a self-selected speed. The subject required an adjustment period of an hour to walk with the final six-bar KAFO prototype. Figure 12(b) provides a comparison of the knee and ankle angular motion, as well as the trajectory of the foot of the user over a complete gait cycle for the following three cases: (1) motion data of the user unassisted, (2) calculated kinematics of the six-bar KAFO linkage, and (3) motion data of the user walking with the final six-bar KAFO prototype. The user's knee ROM with the KAFO was found to be 79 deg, an increase of 22% on the predicted knee ROM for the device. However, this is a significant improvement compared to the reported 40° knee ROM achieved with commercial SC-KAFOs [3]. The user's ankle ROM reduces to 45.89 deg from 52.62 deg with the previous prototype designed. This result provides conditional validation for the authors' hypothesis.

## 4 Conclusions

A two-step design procedure for optimally synthesizing a six-bar knee-ankle-foot-orthosis to produce kinematically accurate human walking motion is presented. The passive six-bar KAFO is designed such that it couples the motion of the knee, ankle, and foot of the user. Preliminary device testing and kinematic evaluation are performed to quantify the results that show the designed passive KAFO can support both flexion and extension of the knee joint during walking. Its kinematic performance is found to be promising, and it demonstrates the feasibility of the concept.

In addition to assessing the device performance from design prospective, preliminary experimental testing with a healthy subject wearing the first and then the second prototype were performed. The main goal was to get a general feedback on the device wearability, through observation and survey-based methods. The preliminary wearability assessment involved an evaluation of the physiological and comfort effects. The selected method for physiological assessment was related to the level of energy spent to operate the device while performing the specific physical training activity. The comfort category assessment referred to localized discomfort due to musculoskeletal loading in a sense of (1) attachment, (2) harm, and (3) movement. Specifically, attachment was related to the level of physical sensation of the device on the body, harm incorporated physical sensation conveying pain, and movement was related to the wearer making conscious modifications/compensations to the movement. The level of the physiological and comfort-related effects ranged from "low" to "extreme." The preliminary evaluation of the device shows promising quantitative results, as it is lighter, easier to operate, and considerably more comfortable than the previous prototype designed.

## Acknowledgment

The authors would like to thank Professor Mark Plecnik, Zonghao "Benjamin" Liu, Hilen Rocha, Abdulsahib Al-Hazza, Abdullaaziz Al-Kharas, Ahmed Shehab, Kevin Masone, and Carresa Brewer for their contributions to this work, as well as NSF Award ID No. 1751770.

## References

- [1] Yakimovich, T., Lemaire, E. D., and Kofman, J., 2006, "Preliminary Kinematic Evaluation of a New Stance-Control Knee-Ankle-Foot Orthosis," *Clin. Biomed.*, **21**(10), pp. 1081–1089.
- [2] Probsting, E., Kannenberg, A., and Zacharias, B., 2017, "Safety and Walking Ability of KAFO Users With the C-Brace® Orthotronic Mobility System, A New Microprocessor Stance and Swing Control Orthosis," *Prosthet. Orthotics Int.*, **41**(1), pp. 65–77.
- [3] Rafaei, M., Bahramizadeh, M., Arazpour, M., Samadian, M., Hutchins, S. W., Farahmand, F., and Mardani, M. A., 2016, "The Gait and Energy Efficiency of Stance Control Knee–Ankle–Foot Orthoses: A Literature Review," *Prosthet. Orthotics Int.*, **40**(2), pp. 202–214.
- [4] McDaid, C., Fayer, D., Booth, A., O'Connor, J., Rodriguez-Lopez, R., McCaughan, D., Bowers, R., Iglesias, C. P., Lalor, S., O'Connor, R. J., Phillips, M., and Ramdharry, G., 2017, "Systematic Review of the Evidence on Orthotic Devices for the Management of Knee Instability Related to Neuromuscular and Central Nervous System Disorders," *BMJ Open*, **7**(9), p. e015927.
- [5] Yakimovich, T., Lemaire, E. D., and Kofman, J., 2009, "Engineering Design Review of Stance-Control Knee-Ankle-Foot Orthoses," *J. Rehabil. Res. Dev.*, **46**(2), pp. 257–267.
- [6] Tian, F., Hefzy, M. S., and Elahinia, M., 2015, "State of the Art Review of Knee–Ankle–Foot Orthoses," *Ann. Biomed. Eng.*, **43**(2), pp. 427–441.
- [7] McMillan, A. G., Kendrick, K., Michael, J. W., Aronson, J., and Horton, G. W., 2004, "Preliminary Evidence for Effectiveness of a Stance Control Orthosis," *JPO J. Prosthet. Orthotics*, **16**(1), pp. 6–13.
- [8] Berkelman, P., Rossi, P., Lu, T., and Ma, J., 2007, "Passive Orthosis Linkage for Locomotor Rehabilitation," IEEE 10th International Conference on Rehabilitation Robotics, *ICORR 2007*, Noordwijk, The Netherlands, June 13–15, pp. 425–431.
- [9] Agrawal, S. K., Banala, S. K., Fattah, A., Sangwan, V., Krishnamoorthy, V., Scholz, J. P., and Hsu, W., 2007, "Assessment of Motion of a Swing Leg and Gait Rehabilitation With a Gravity Balancing Exoskeleton," *IEEE Trans. Neural Syst. Rehabil. Eng.*, **15**(3), pp. 410–420.
- [10] Ji, Z., and Manna, Y., 2008, "Synthesis of a Pattern Generation Mechanism for Gait Rehabilitation," *ASME J. Med. Devices*, **2**(3), p. 031004.
- [11] Tsuge, B. Y., and McCarthy, J. M., 2015, "Synthesis of a 10-Bar Linkage to Guide the Gait Cycle of the Human Leg," *ASME* Paper No. DETC2015-47723.
- [12] Shao, Y., Xiang, Z., Liu, H., and Li, L., 2016, "Conceptual Design and Dimensional Synthesis of Cam-Linkage Mechanisms for Gait Rehabilitation," *Mech. Mach. Theory*, **104**, pp. 31–42.
- [13] Bapat, G. M., and Sujatha, S., 2017, "A Method for Optimal Synthesis of a Biomimetic Four-Bar Linkage Knee Joint for a Knee-Ankle-Foot Orthosis," *J. Biomimetics, Biomater. Biomed. Eng.*, **32**, pp. 20–28.
- [14] Foster, R., and Milani, J., 1979, "The Genucentric Knee Orthosis - A New Concept," *Orthotics Prosthet.*, **33**(2), pp. 31–44.
- [15] Walker, P., Kurosawa, H., Rovick, J., and Zimmerman, R., 1985, "External Knee Joint Design Based on Normal Motion," *J. Rehabil. Res. Dev.*, **22**(1), pp. 9–22.
- [16] Townsend, J., and Knecht, S., 2004, "Tension Assisted Ankle Joint and Orthotic Limb Braces Incorporating Same," U.S. Patent No. 6,752,774.
- [17] Radcliffe, C., 1994, "Four-Bar Linkage Prosthetic Knee Mechanisms: Kinematics, Alignment and Prescription Criteria," *Prosthetics Orthotics Int.*, **18**(3), pp. 159–173.
- [18] Plecnik, M. M., and McCarthy, J. M., 2016, "Computational Design of Stephenson II Six-Bar Function Generators for 11 Accuracy Points," *ASME J. Mech. Rob.*, **8**(1), p. 011017.
- [19] Plecnik, M. M., and McCarthy, J. M., 2016, "Controlling the Movement of a TRR Spatial Chain With Coupled Six-Bar Function Generators for Biomimetic Motion," *ASME J. Mech. Rob.*, **8**(5), p. 051005.
- [20] Ghosh, S., Robson, N., and McCarthy, J., 2017, "Design of Wearable Lower Leg Orthotic Based on Six-Bar Linkage," *ASME* Paper No. DETC2017-67837.
- [21] Smaili, A. A., Diab, N. A., and Atallah, N. A., 2005, "Optimum Synthesis of Mechanisms Using Tabu-Gradient Search Algorithm," *ASME J. Mech. Des.*, **127**(5), pp. 917–923.
- [22] Tsuge, B. Y., Plecnik, M. M., and McCarthy, J. M., 2016, "Homotopy Directed Optimization to Design a Six-Bar Linkage for a Lower Limb With a Natural Ankle Trajectory," *ASME J. Mech. Rob.*, **8**(6), p. 061009.
- [23] Dibakar, S., and Mruthyunjaya, T., 1999, "Synthesis of Workspaces of Planar Manipulators With Arbitrary Topology Using Shape Representation and Simulated Annealing," *Mech. Mach. Theory*, **34**(3), pp. 391–420.
- [24] Robson, N., and Ghosh, S., 2016, "Geometric Design of Planar Mechanisms Based on Virtual Guides for Manipulation," *Robotica*, **34**(12), pp. 2653–2668.
- [25] Bates, D. J., Hauenstein, J. D., Sommese, A. J., and Wampler, C. W., 2013, *Numerically Solving Polynomial Systems With Bertini*, SIAM Press, Philadelphia, PA.
- [26] Ghosh, S., Robson, N., and McCarthy, J., 2017, "Development of Customized Orthotics Based on Lower-Leg Anthropometric Data and Task," *International Conference on Applied Human Factors and Ergonomics*, Springer, Los Angeles, CA, July 17–21, pp. 54–63.
- [27] Rao, S. S., 2009, *Engineering Optimization: Theory and Practice*, John Wiley & Sons, Hoboken, NJ.
- [28] Wolfram, S., 2003, *The Mathematica Book*, 5th ed., Wolfram Media, Champaign, IL.